Mon. Not. R. Astron. Soc. **264,** 181–190 (1993)

Vela X-1 and its missing third harmonic

Mauro Orlandini★†
Laboratory for High Energy Astrophysics, Code 666, NASA/Goddard Space Flight Center, Greenbelt, MD 20771, USA

Accepted 1993 February 25. Received 1993 February 19; in original form 1992 December 9

ABSTRACT

In our analysis of 13 *HEAO 1* A2 pointed observations of the X-ray binary pulsar Vela X-1, we have confirmed that its third pulsation harmonic is almost missing (the peak is ~ 2–3σ above the continuum, with a drop of power of ~ 2 orders of magnitude with respect to the power present in the second harmonic). This feature is intrinsic to Vela X-1 and is independent of the timing resolution and the energy, although the harmonic content in the MED and HED data is quite different, because of the different pulse shape in the two energy bands. This drop has already been observed by the *EXOSAT* (although not pointed out) and the *BBXRT* observatories, and to our knowledge no other X-ray binary pulsar is known to show this peculiarity. For the high-energy data, we find a possible explanation of the phenomenon in the geometrical configuration of emission from radiating slabs at the polar caps, modelled according to Leahy. In order to model the low-energy harmonic content, we develop a phenomenological model of the Vela X-1 pulse profile in terms of two signals: a carrier with a double-peak structure, and a modulation with a five-peak structure. The harmonic content computed in the model is in agreement with the observations. Some possible physical interpretations of the two signals are discussed.

Key words: binaries: close – pulsars: individual: Vela X-1 – X-rays: stars.

1 INTRODUCTION

The X-ray binary system Vela X-1 consists of a neutron star, spinning at a period of about 283 s (McClintock et al. 1976), and a supergiant star of spectral type B0 (Hutchings 1974), which emits a strong stellar wind that, by accretion, powers the X-ray emission. The system shows an X-ray eclipse which lasts about 1.7 d (Avni 1976). The orbital parameters of this system leave no doubt that the supergiant does not fill its Roche lobe (Rappaport, Joss & Stothers 1980), therefore the main accretion path on to the neutron star occurs directly from the stellar wind.

In this paper we discuss a result obtained during our temporal analysis of 13 observations of Vela X-1 observed by the A2 experiment aboard the X-ray satellite *HEAO 1*, namely the absence of the third harmonic of pulsation. This is a characteristic of the emission from Vela X-1. It was present in the *EXOSAT* observations [see table 2 of Raubenheimer & Ögelman (1990)] and also in the *BBXRT* observation (Soong, private communication). To our knowledge, a similar feature has not been reported for any other X-ray binary pulsar. We have, furthermore, browsed the *EXOSAT* data base archive in order to extract the harmonic content from data for other pulsars. We did not find any strange behaviour and/or the absence of any harmonic in the sample of observations we analysed.

After the presentation of the results of the data analysis in Section 2, in Section 3 we discuss the harmonic content of the high-energy data in the framework of the analytical pulsar emission model by Leahy (1990, hereafter L90). We generalize the L90 model for the high-energy emission from Vela X-1 and show that the missing harmonic can be explained in terms of the geometrical configuration of emission of this system. We then discuss the more complex pulse shape of the lower energy data from Vela X-1, and show that it can be described in terms of two different modulations from the polar caps. This model successfully predicts the absence of the third pulsation harmonic. Section 4 contains our conclusions.

2 OBSERVATIONS

For our analysis we have used 13 pointed observations obtained by the A2 experiment aboard *HEAO 1*. The A2 experiment consisted of six gas proportional counters sensitive to different energy bands [see Rothschild et al. (1979) for

★NAS/NRC Resident Associate.
†Present address: TESRE Institute, via de' Castagnoli 1, 40126 Bologna, Italy.

details]. We have utilized data from both the MED, an argon-filled detector that is sensitive in the 1.5–20 keV energy band, and the HED III, a xenon-filled detector sensitive in the 2.5–60 keV energy band. Both detectors had an effective area of ~ 800 cm^2. We used data with 80-ms timing resolution from each detector. These rates included all good events in the detector between the lower and upper discriminators. Thus each detector rate is an integral over the spectrum, weighted by the response function. For the MED data the average energy, assuming a hard pulsar spectrum, is ~ 4 keV, while it is ~ 12 keV for the HED data.

The journal of observations is shown in Table 1 (HED data were not available for all the observations). In the first observation we analysed (observation 508), Vela X-1 was in eclipse. The observations are spread over the entire orbit of 8.96 d (we have used the orbital parameters given by Rappaport, Joss & Stothers 1980). The real length of each observation is reduced because of South Atlantic Anomaly passages, Earth occultations, and some data losses.

We performed the analysis on data with 80-ms timing resolution and on data rebinned at 4.96 s. Because the main gaps between data are of the order of 2500–2600 s, we used intervals of 32 768 and 512 points for the 80-ms and 4.96-s data, respectively, in the computation of power spectrum density estimates (PSDs) by means of fast Fourier transform algorithms. In this way we eliminate the spurious effect due to the interruptions in the data. Each PSD has been normalized in such a way that the (white) Poissonian noise has a value of a power of 2.

We show in Fig. 1 the PSD of observation 715 computed with MED data binned at 4.96 s. The peaks due to the harmonics of pulsation are clearly visible (and are marked by dotted lines). In this particular case, at least the first 15 harmonics are present. In other observations, the number of harmonics clearly identifiable is different, ranging from 9 to 20.

In Fig. 2 we show the PSD computed with the 4.96-s HED data for observation 718. The harmonic content is quite different from that shown by the low-energy data. This is due to the fact that the shape of the pulse profile changes from a five-peak structure at low energy to a double-peak structure at higher energies, which makes the second harmonic the more prominent feature in the HED power spectra. The number of harmonics is smaller than the number observed in the MED PSDs, ranging from 9 to 13.

There are two features common to all the observations.

(i) The third harmonic is practically missing. This result is independent of the energy band. The third-harmonic peak is $\sim 2\sigma$ above the continuum for the MED data, and $\sim 3\sigma$ above the continuum for the HED data. The power in the peak of the third harmonic is about 2 orders of magnitude less than the power present in the second one (the most prominent feature in both the MED and the HED data).

(ii) There is a dramatic drop of power after the seventh harmonic (note in Figs 1 and 2 the different scales for power in the two panels).

For a quantitative analysis, we show in Fig. 3 the power present in the first four harmonics of three HED observations of Vela X-1. The harmonic content has been computed from the Fourier expansion that fits the observed pulse profiles, normalized in the interval 0–1. We can see that the third harmonic is very variable (more than 1 order of magnitude from observations 715 to 716), while the other three har-

Table 1. Journal of observations for the 13 *HEAO 1* A2 observations of Vela X-1.

Obs ID	Date (1978)	Mid Date[a]	Orbital Phase	Obs Length (s) total	Obs Length (s) net	⟨*I*⟩ MED (Cnts/s)	⟨*I*⟩ HED (Cnts/s)
508	May 23	3652.02	0.872–0.895	18151.60	7172.56	1.92 ± 0.04	—
510	May 25	3654.01	0.092–0.118	19865.52	10320.16	47.64 ± 0.07	—
512	May 27	3656.01	0.315–0.341	19824.56	10606.56	103.63 ± 0.10	—
699	Nov 30	3843.22	0.207–0.215	6348.72	3030.72	31.69 ± 0.12	—
706	Dec 07	3850.24	0.975–0.014	30392.24	15685.92	65.39 ± 0.07	14.32 ± 0.03
712	Dec 13	3855.91	0.599–0.653	41438.00	14812.72	43.73 ± 0.06	13.15 ± 0.03
715	Dec 16	3859.16	0.963–0.015	39587.12	19637.68	51.64 ± 0.06	13.99 ± 0.03
716	Dec 17	3860.68	0.138–0.178	30515.12	13474.64	81.23 ± 0.09	17.85 ± 0.04
718	Dec 19	3862.07	0.287–0.341	41492.40	22936.16	76.12 ± 0.06	26.26 ± 0.03
719	Dec 20	3863.47	0.443–0.497	41492.20	10320.00	54.17 ± 0.08	13.81 ± 0.04
721	Dec 22	3865.00	0.613–0.667	41492.40	21133.28	45.44 ± 0.05	10.11 ± 0.02
724	Dec 25	3868.30	0.996–0.021	19455.92	7371.44	40.02 ± 0.08	9.55 ± 0.04
730	Dec 31	3873.91	0.605–0.663	44206.00	19913.28	24.52 ± 0.04	10.20 ± 0.03

[a]Date in JD − 244 0000.
Orbital phases are computed from the ephemeris given by Rappaport, Joss & Stothers (1980). Each observation contains data gaps due to the South Atlantic Anomaly passages, Earth occultations and data losses due to telemetry: this is the reason why we give the total span and the net length of each observation. For the first four observations, HED data are not available.

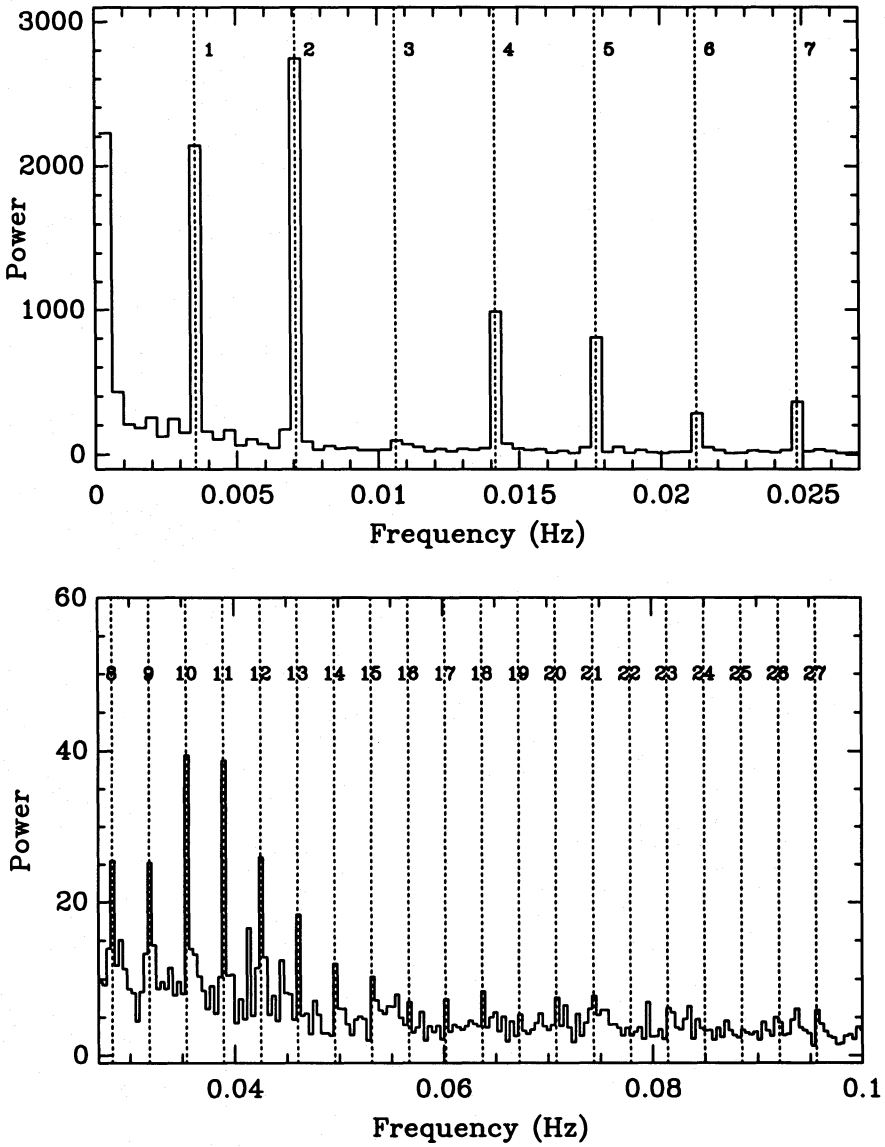

Figure 1. PSD computed for observation 715 using MED data rebinned at 4.96 s. The peaks due to the pulsation are clearly visible. Note the missing third harmonic and the dramatic drop in power beyond the seventh harmonic (lower panel). The peak of the third harmonic is $\sim 2\sigma$ above the continuum level.

monics show lower variability. We do not find any correlation between the harmonic content and the X-ray luminosity.

3 DISCUSSION

In trying to explain the absence of the third pulsation harmonic in the coherent emission from Vela X-1, it is difficult to think of a physical process that is able to discriminate a peculiar frequency so strongly and then to drop it. The most likely origin of this phenomenon lies in the geometry of emission.

The variation of the observed X-ray flux as a function of the pulse phase is due to two different processes: the first is the intrinsic angular dependence of the emission pattern (which is described in a reference frame fixed to the neutron star surface); and the second is the variation of the X-ray intensity along the line of sight, a purely geometrical phenomenon that is related to the rotation of the neutron star, and which depends on the angle between the neutron star magnetic axis and the spin axis, θ_m, and the angle between the line of sight and the rotation axis, θ_r. Furthermore, the pattern in the neutron star frame of reference could also be affected by the rotation with respect to the accretion flow.

Although the third harmonic shows a dramatic drop in both the MED and the HED data, the harmonic content is quite different in the two energy bands. For this reason we will discuss separately the results obtained from the two kinds of data.

3.1 HED observations

With respect to the intrinsic emission pattern, numerical calculations are available for the angular and energy dependences of the emitted X-rays [see e.g. Mészáros & Nagel

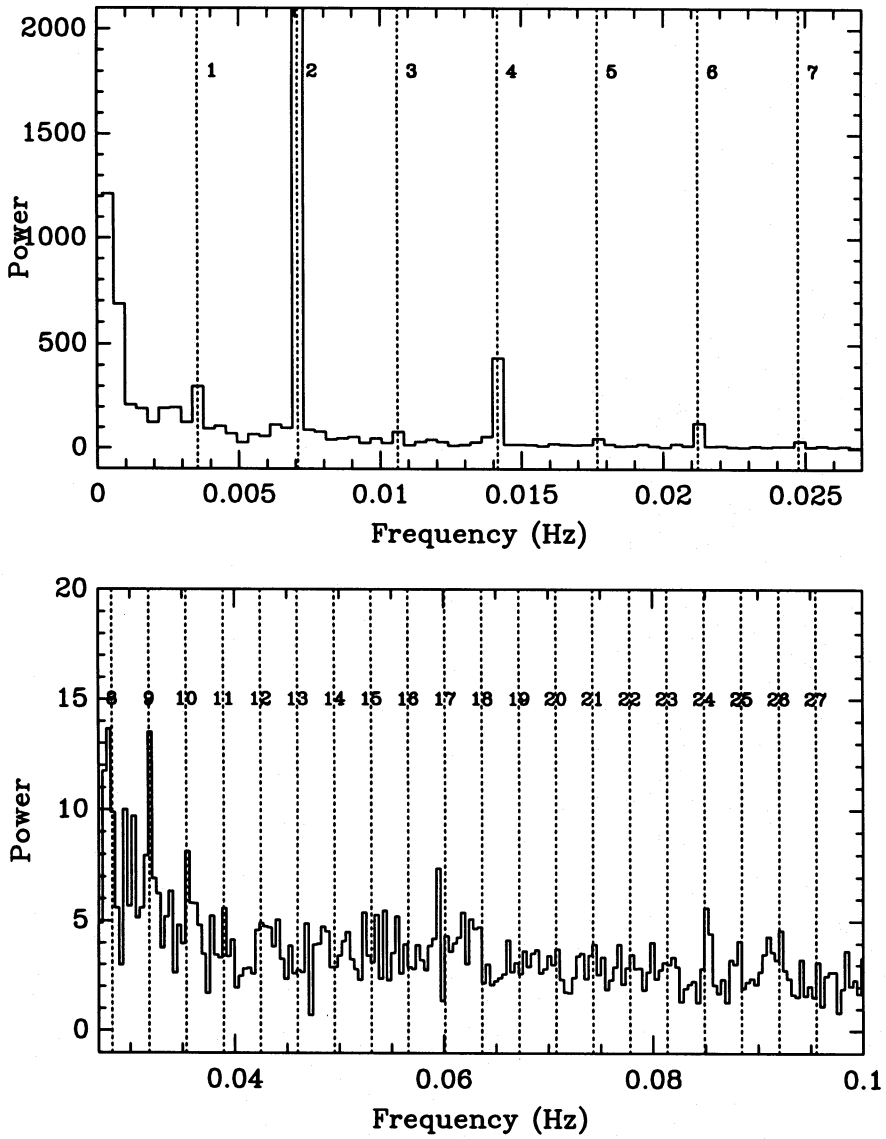

Figure 2. PSD computed for observation 718 using HED data rebinned at 4.96 s. The peaks due to the pulsation are clearly visible. The most prominent feature is the second harmonic, because of the double-peak structure of the pulse profile in this energy band (its value is ~4100 power units, off the scale in the upper panel). The third harmonic is still very low (~3σ above the continuum). As in the case of the MED data, there is a dramatic drop in power beyond the seventh harmonic (lower panel). Note that the power present in the odd harmonics is less than the power present in the even harmonics. This is what is expected from expanding equation (1) in terms of even powers of cos θ and putting one geometrical angle close to $\pi/2$.

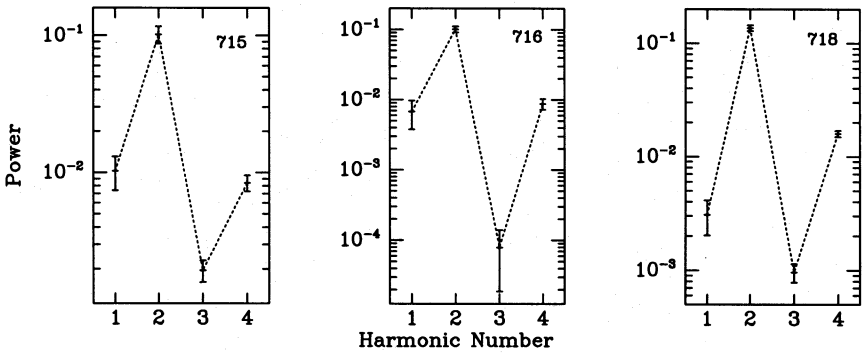

Figure 3. The power present in the first four harmonics for three HED observations of Vela X-1: 715, 716 and 718. The harmonic content has been computed from the observed pulse profiles, normalized in the interval 0–1, by computing the Fourier expansion that fits the pulse shapes. In all the HED observations the first four harmonics are almost constant except the third, which shows a more than 1 order of magnitude difference between observations 715 and 716. We did not find any correlation between the harmonic content and the X-ray luminosity.

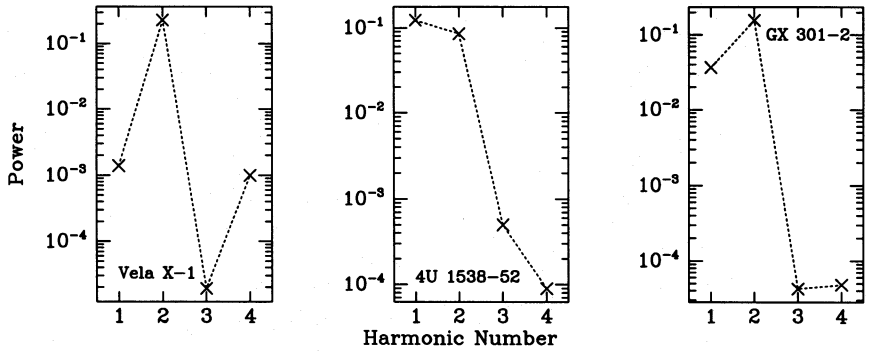

Figure 4. The power present in the first four harmonics, computed from the modelled flux distribution given by L90, for the wind-fed X-ray pulsars Vela X-1, 4U 1538 − 52 and GX 301 − 2. Before performing the Fourier analysis, the modelled pulse profile was normalized in the interval 0–1. Vela X-1 is the only source, among those given by L90, that shows a missing third harmonic.

(1985) and references therein], and attempts have been made to model the dependence with some simple analytical functions (Leahy 1990, 1991). With the analytical formulation of L90, it is possible to reconstruct the variation of the X-ray flux from the neutron star, originating from radiating slabs at the magnetic poles, as a function of the pulse phase φ [the assumption of a pencil-beam emission pattern is justified by the low X-ray luminosity of Vela X-1 (Basko & Sunyaev 1976)]. The variation also depends on the dimensions of the emitting region on the neutron star surface, and on the energy of the X-ray radiation emitted. By adopting an annular-shaped emitting region[1] defined by two angles α and β (measured from the magnetic field axis in a reference frame with the z-axis along the magnetic field axis; $\alpha < \beta < \pi/2$), we find that the flux from the neutron star surface as a function of the angle θ between the line of sight and the magnetic axis can be approximated by

$$f(\theta) = a\cos^4\theta + b\cos^2\theta + c \qquad (1)$$

(L90), where $\cos\theta$ is given by

$$\cos\theta = \cos\theta_m \cos\theta_r + \sin\theta_m \sin\theta_r \cos\varphi, \qquad (2)$$

and the coefficients a, b and c are functions of α, β and the X-ray energy emitted.

The main problem relating to the use of equation (1) is the fact that it does not predict any harmonic beyond the fourth, while in Figs 1 and 2 we clearly see that more harmonics are present in observations of Vela X-1. We will discuss this approximation later, when we will generalize equation (1) to a general expansion of $f(\theta)$ in terms of powers of $\cos^{2n}\theta$. For the moment, let us use equation (1) as a zeroth-order approximation. We shall see below that, even with only three terms in equation (1), Leahy's model is able to describe qualitatively the amount of power present in the first four harmonics of Vela X-1 quite well.

For the third pulsation harmonic to be missing in the Fourier expansion of the pulse profile in equation (1), it is necessary either that a is zero, or that one of the geometrical angles θ_r or θ_m is close to $\pi/2$. Because the fourth harmonic is not missing (see Figs 1 and 2), we cannot have $a = 0$, so we prefer the hypothesis θ_r or $\theta_m \sim \pi/2$.

To test the hypothesis that the missing third harmonic is a result of the geometrical configuration of emission, we computed the Fourier expansions that fit the flux distribution obtained by L90 for his sample of pulsars. For Vela X-1 the third harmonic shows a more marked decrease in power than it does for the modelled flux from other pulsars, and so seems to be intrinsic to the geometry of emission of Vela X-1. In Fig. 4 the power present in the first four harmonics is shown for the modelled flux from the wind-fed X-ray pulsars Vela X-1, GX 301 − 2 and 4U 1538 − 52.

The observed harmonic content in the first four pulsation harmonics in Vela X-1 (Fig. 3) is in reasonably good qualitative agreement with the harmonic content predicted by Leahy's model (Fig. 4). Despite the approximation made in the model, i.e. the description of only four harmonics, it is able to predict the drop in power corresponding to the third harmonic. The model does not account for the exact amount of power present in each harmonic, but the variability we observe in the peaks from observation to observation is a factor that surely influences these quantities.

In order to check the approximation involved in equation (1), we generalized the expansion of $f(\theta)$ by assuming an arbitrary number of even powers of $\cos\theta$ (see the Appendix for details). By assuming that one of the geometrical angles is close to $\pi/2$ (we will label the two geometrical angles θ_1 and θ_2, because they are interchangeable in the model; see equation 2), we can obtain an analytical expression for the power present in each pulsation harmonic as a function of the coefficients of the expansion (which depends on the dimensions of the polar cap), the other geometrical angle, and the parameter ξ, defined as $(\pi/2 - \theta_{1,2})$. From equation (A9) we can see that the power present in the odd harmonics is a quantity of the second order in ξ, while that present in the even harmonics is linear and quadratic. This means that the even harmonics must be higher than the odd harmonics. How much lower the odd harmonics are with respect to the even ones is a strong function of the coefficients of the expansion. In any case, the HED power spectra of Vela X-1 show that the even harmonics are higher than the odd ones, and this is in agreement with the hypothesis of one of the geometrical angles being close to $\pi/2$ (see Fig. 2).

[1] In the following we will discuss the case of aligned polar caps. The most general case of offset emitting regions (which can also have different areas) was treated by Leahy (1991), who showed that Vela X-1 does not require an offset angle to fit the observed asymmetric pulse profiles, but only two different areas for the polar caps.

We furthermore computed the values of the geometrical angles for which the power present in the third harmonic, P_3, is less than the power present in the fourth, P_4 (always according to the model by L90), and the result is shown in Fig. 5, together with the geometrical angles given by L90 for 15 binary pulsars. The open circles and triangles represent the symmetric solution with respect to the line $\theta_2 = \theta_1$. We mark with a cross the solution for Vela X-1. As we can see, this solution is in agreement with a missing third harmonic, and corresponds to one of the geometrical angles being close to $\pi/2$.

From a theoretical point of view, this interpretation is in agreement with the Kanno (1980) model of the energy dependence of the Vela X-1 pulse profile, in which the variability is explained in terms of the geometry of emission. The physical process responsible for the variability is an opacity dominated by the Thomson scattering of weakly dispersive electrons in the strongly magnetized atmosphere of the neutron star. In this model, the formation of up to six peaks in the pulse profile can be achieved if $|\theta_1 - \theta_2| \lesssim 15°$ and $|\theta_1 + \theta_2| \gtrsim 140°$, i.e. either θ_1 or θ_2 has to be close to $\pi/2$ (see also Mészáros & Bonazzola 1981).

In Fig. 5 we mark with triangles the X-ray binary pulsars that show an eclipse. The presence of an eclipse constrains the inclination of the orbital plane to values very close to $\pi/2$ [for Vela X-1 it is $i > 74°$ (Avni 1976)]. The two sources that are very close to the $P_3 = P_4$ curve [4U 1258 − 62 (Corbet et al. 1986) and GX 301 − 2 (Sato et al. 1986)], although they do not show an eclipse, are thought to have very large inclination angles. This, together with the probable condition of coplanarity of the two components of the binary system (i.e. the equatorial planes of the two stars coincide with the orbital plane), means that it is likely that the geometrical angle close to $\pi/2$ can be identified with the angle between the spin axis and the line of sight, i.e. θ_r. Indeed, the time-scale necessary to align the spin axes of the two stars and make them perpendicular to the orbital plane is shorter than the tidal time-scale necessary to synchronize the orbit (Hut 1981). L90 arrived at the same conclusion, $\theta_1 \equiv \theta_r$, from the distribution of θ_1 and θ_2 among the X-ray pulsars.

The fact that almost all the other pulsars belong to the θ_1–θ_2 region for which the third harmonic is relatively large, so that both angles are farther from $\pi/2$, could possibly be explained if the angle $\sim \pi/2$ is θ_m, i.e. could be explained in terms of misalignment between the magnetic and spin axes. The alignment torque is due to the magnetic dipole radiation reaction that causes the decrease of θ_m (Davis & Goldstein 1970). It has been shown by Lyne & Manchester (1988) that in *isolated radio* pulsars the distribution of θ_m is almost uniform for young pulsars, while old pulsars show aligned axes. The time-scale for alignment is of the order of 10^7 yr, which is longer than the expected lifetime of X-ray binary

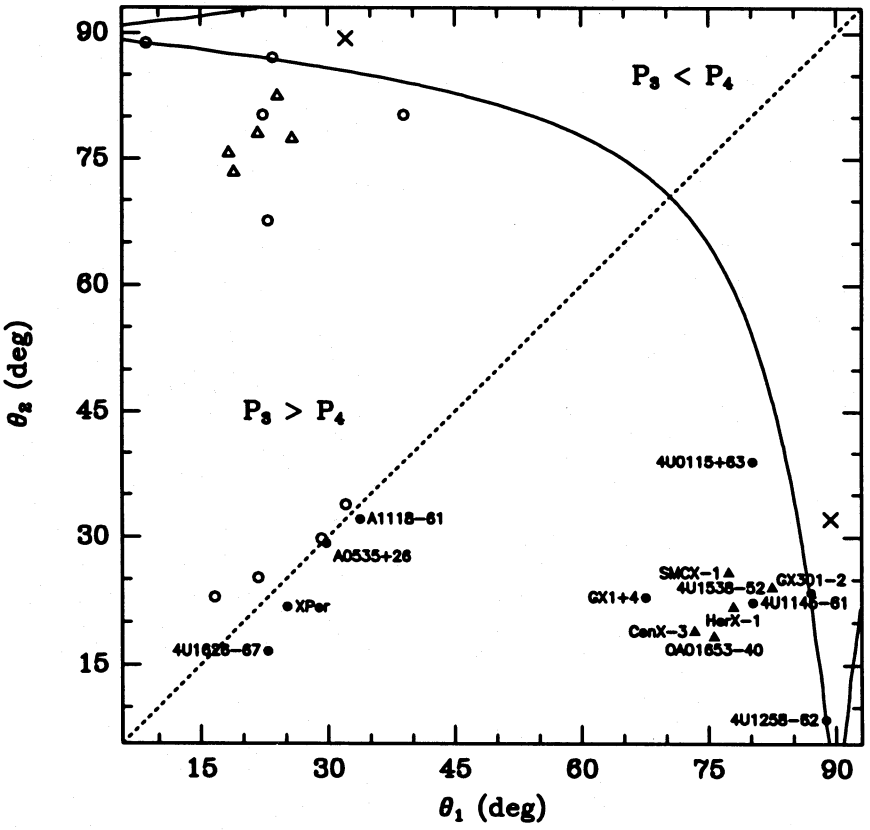

Figure 5. This curve represents the values of the geometrical angles θ_1 and θ_2 for which the power present in the third harmonic, P_3, and that present in the fourth, P_4, are equal. Here we show only the curve for $0 < \theta_{1,2} < \pi/2$, because the curve is symmetric with respect to the lines $\theta_{1,2} = \pi/2$. The flux distribution has been modelled according to L90. The crosses represent the values of θ_1 and θ_2 given by L90 for Vela X-1, and belong to the θ_1–θ_2 region for which $P_3 < P_4$. The filled circles represent the geometrical angles for the other L90 X-ray pulsars, and the filled triangles represent the pulsars that show an X-ray eclipse (the open symbols represent the symmetric solution with respect to the line $\theta_2 = \theta_1$). The curve is almost independent of the dimensions of the polar cap.

pulsars [of the order of 10^5 yr (Hellings & de Loore 1986)]. If this explanation were correct, Vela X-1 would be one of the youngest X-ray binary pulsars in the group of X-ray pulsars analysed by L90, and this would be in agreement with the current evolutionary scenario for massive X-ray binaries: X-rays powered by stellar wind accretion are most likely to be present in young systems, while Roche-lobe overflow is expected in the oldest X-ray binary pulsars [see Hellings & de Loore (1986) and references therein].

3.2 MED data

In the previous section we have seen that Leahy's model is able to describe the high-energy, double-peaked pulse profile of Vela X-1 if one of the geometrical angles of emission is close to $\pi/2$.

Leahy's model is, however, not adequate to model the five-peak structure of the pulse profile observed at lower energy, because the approximation of equation (1) (and its generalization, equation A1) implies a description of the pulse shape in terms of even functions, which is not possible for the odd-peaked MED pulse profile. Indeed, the harmonic content in this energy band does not show the decrease in the odd harmonics observed for the HED data.

In order to build a phenomenological model of the Vela X-1 pulse profile, we must also take into consideration the morphological properties of the MED and HED pulses. The MED Vela X-1 pulse shape shows a five-peak structure in which two 'main peaks' are present (these peaks can be identified with the emission from the two polar caps). The minimum between the two peaks is stable in phase, and is located at about phase 0.55. On the lower main peak three subpeaks are present, while on the higher main peak two subpeaks are present. The HED pulse profile of Vela X-1 shows a double-peak structure. The minimum between the two peaks is stable in phase, and located at approximately the same position as that in the MED data.

To model the presence of a double-peak structure in both pulse profiles, we constructed a phenomenological model of the MED Vela X-1 pulse profile in which the double-peak structure is described as the result of two separate signals: a *carrier* with a double-peak structure, and a *modulation* formed by three peaks plus another two. We can explain the difference between the pulse profiles in the two energy bands by postulating that for the HED observations the carrier only is observed, while for the low-energy data both the signals are present.

We computed the resulting modulation for both a sum and a product (i.e. an amplitude modulation) of the two underlying signals, and also computed the Fourier expansion that fits the pulse profile thus obtained. We varied the free parameters (described in Fig. 6) in order to obtain a harmonic content of the same type as we observe in the real data; our results are shown in Fig. 7. As can be seen, we obtain a reasonably good qualitative agreement with the observations for both the models: both predict strong drops in the third

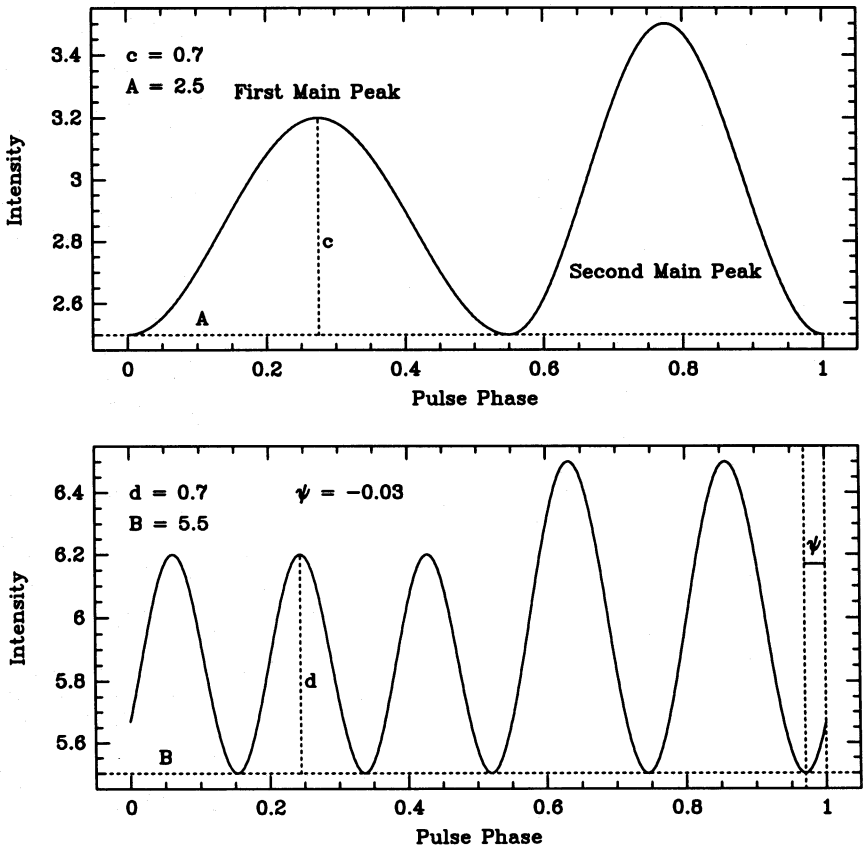

Figure 6. Description of the free parameters of our phenomenological model for the Vela X-1 pulse profile. The two parameters c and d correspond to the heights of the second main peaks normalized to the heights of the first main peaks in the carrier and the modulation, respectively. The two values A and B correspond to the minimum in the two signals, and ψ is the offset phase angle between the two signals.

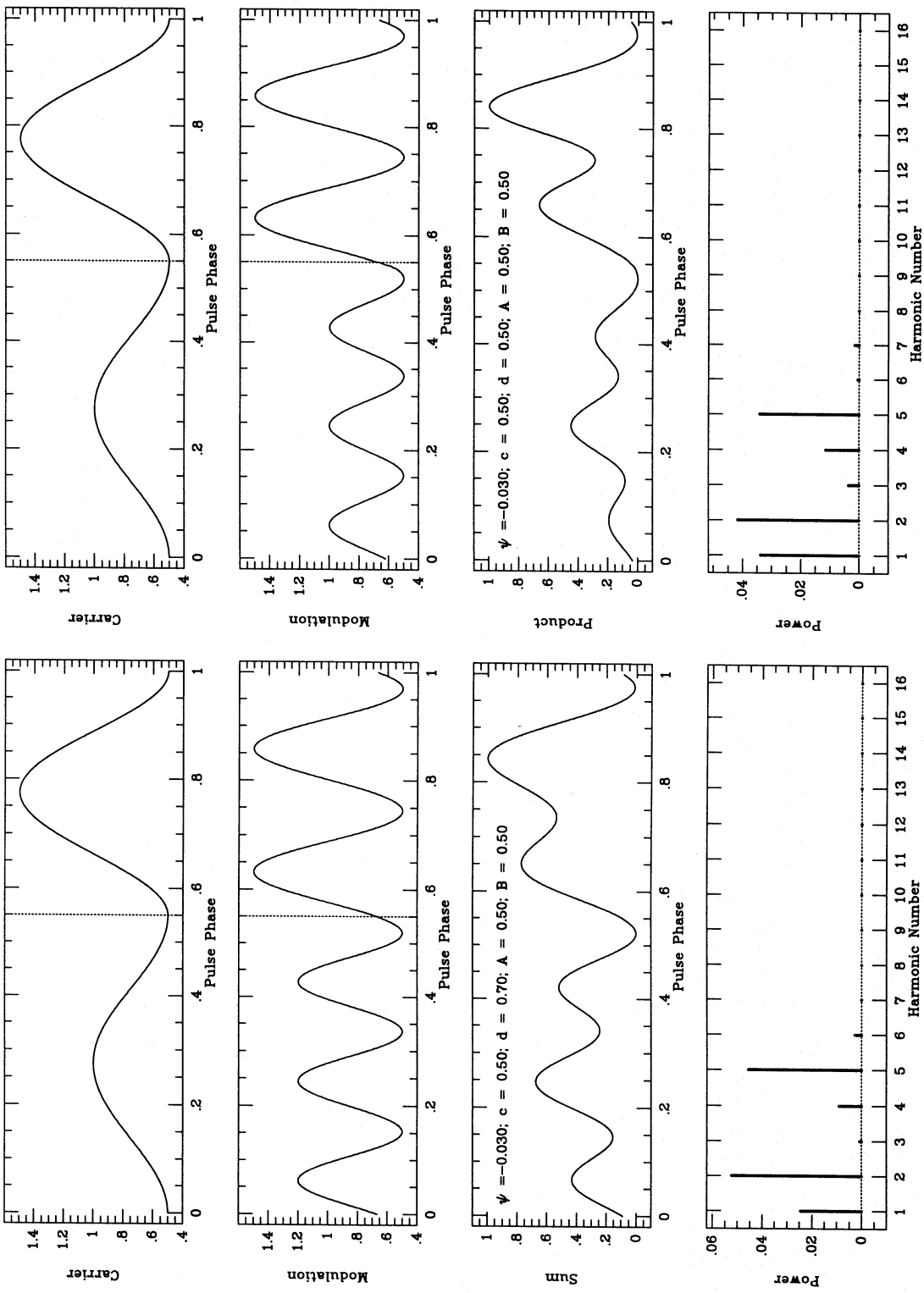

Figure 7. Harmonic analysis of our phenomenological model for the Vela X-1 pulse profile. In the upper four panels, the carrier and the modulation signals are shown. In the two panels beneath we show on the left the sum and on the right the product (i.e. an amplitude modulation) of the two signals, and in the bottom two panels the harmonic content is presented for the first 16 harmonics. For both the models a solution that is able to fit the observed whole harmonic content does not exist. The drop in power in the third harmonic and after the seventh is, however, quite well described.

pulsation harmonic and after the seventh pulsation harmonic (although it was not possible to find a solution able to give an acceptable χ^2 for a fit to the whole harmonic content observed for Vela X-1).

The next step is to give a physical meaning to the two underlying signals. We have already shown that the L90 model is able to describe the *carrier* quite well. The carrier could be interpreted physically in terms of the emission from the two polar caps of Vela X-1.

It is more of a challenge to obtain a physical interpretation of the *modulation* signal. We can think of two different processes: a structure in the emission region (Lyubarskii & Sunyaev 1988; Burnard, Arons & Klein 1991), or some inhomogeneity that orbits steadily above the polar caps and causes absorption of low-energy photons (Nagase et al. 1986). In the case of emission from a hollow column, the two subpeaks observed in the second main peak could be interpreted as the passage of the line of sight across the walls of the column. The observed asymmetry in the two hotspots, i.e. the presence of a different number of subpeaks, might be explained in terms of a different viewing angle of the emitting regions, but examination of quantitative models of this phenomenon is beyond the scope of this paper.

Another possibility is the presence of cold material steadily orbiting above the polar caps and obscuring the low-energy photons emitted from the neutron star. The problem with this interpretation is that these blobs must possess strong stability in the phase of their orbit about the neutron star in order to explain the stability of the MED pulse profile.

This problem could be solved by the presence of an accretion disc, the inner edge of which could shade the emitting regions [a similar interpretation has been invoked in order to explain the pulse profile of Her X-1 (Sheffer et al. 1992)]. An accretion disc in Vela X-1 has already been discussed fully by Börner et al. (1987); the main problem connected with this model is the very high neutron star magnetic field necessary for disc formation – between 10^{13} and 10^{14} G.

4 CONCLUSIONS

We have seen that there is a notable harmonic content in the data of many observations of Vela X-1, despite the variability of the pulse profile. The absence of the third harmonic of pulsation is a *clear* signature of the coherent emission from this object.

For the HED data, we have shown that the missing third harmonic can be explained in terms of the geometrical configuration of emission from radiating slabs at the magnetic poles of the neutron star. This interpretation is also in agreement with the theoretical model of Kanno (1980), which shows that the frequency dependence of the Vela X-1 pulse profile can be explained in terms of an opacity dominated by Thomson scattering by strongly magnetized but only weakly dispersive electrons in the neutron star magnetosphere, if one of the geometrical angles is close to $\pi/2$.

The identification of θ_r with an angle close to $\pi/2$ would explain why all the X-ray pulsars that show an eclipse have one geometrical angle much higher than the other. This would correspond to the spin axis of the neutron star being almost perpendicular to the orbital plane of the Vela X-1 system, a very likely condition (Hut 1981). In support of this hypothesis is the fact that three of the four sources that lie close to the line $\theta_2 = \theta_1$ have inclination angles much smaller than $\pi/2$. The two sources that may not fit this interpretation are X Persei ($i \approx 80°$, Kemp & Barbour 1983) and 4U 1145 − 61 ($i \lesssim 45°$, Janot-Pacheco, Chevalier & Ilovaisky 1982), and for both these sources very long orbital periods and wide orbits have been suggested. In the framework of this interpretation, we predict that 4U 0115 + 63, OAO 1653 − 40 [which has very recently been found to show an X-ray eclipse (Chakrabarty et al. 1993)] and GX 1 + 4 have inclination angles close to $\pi/2$. With this interpretation, the absence of the third harmonic in Vela X-1 is 'accidental' due to the high value of i.

Although less likely, the low value of the third pulsation harmonic could be explained in terms of a near-perpendicularity between the spin and the magnetic axes. This could occur in a very young neutron star in which the alignment torque has not yet been successful in aligning the two axes. Although, in the current evolutionary model of high-mass X-ray binary pulsars, wind-fed systems are thought to be the youngest ones, there is a problem with this explanation in that a 'young' system such as A0535 + 26 lies very far from the region of near-perpendicularity between the two axes. On the other hand, the 'old' system 4U 1626 − 67 has one of the smallest values of θ_m.

To describe the harmonic content of the MED data, we have built a phenomenological model of its pulse profile and have shown that we can keep the power of the third harmonic low by describing the emission from the polar caps as the result of two signals: a carrier, which is present for both the energy ranges, and a modulation, which is characteristic of the low-energy data. While the carrier can easily be identified as the emission from the two polar caps, the modulation has no simple physical explanation. A structure in the emitting region, inhomogeneous blobs of matter orbiting steadily above the neutron star polar caps, or the presence of an accretion disc which shades the emitting regions could effect such a modulation.

An important effect that is not taken into account in the Leahy model is the bending of the emitted light due to the gravitational field of the neutron star. This general relativistic effect, which has been considered by Pechenick, Ftaclas & Cohen (1983), allows regions of the neutron star that are hidden from the observer in the non-relativistic case to be instead visible because of the curvature of space-time. The amount of light deflection for a typical neutron star is ~ 12° (Pechenick, Ftaclas & Cohen 1983; Ftaclas, Kearney & Pechenick 1986). Because of uncertainties in the theory of X-ray scattering through a strongly magnetized plasma (on which the Leahy model is based), this effect cannot be clearly represented. It should, however, be taken into account in building a model that fits the observed pulse profiles.

ACKNOWLEDGMENTS

The author would like to thank Jean H. Swank for a careful reading of the manuscript and helpful comments.

REFERENCES

Avni Y., 1976, ApJ, 209, 574
Basko M. M., Sunyaev R. A., 1976, MNRAS, 175, 395
Börner G., Hayakawa S., Nagase F., Anzer U., 1987, A&A, 182, 63
Burnard D. J., Arons J., Klein R. I., 1991, ApJ, 367, 575

Chakrabarty D. et al., 1993, ApJ, 403, L33
Corbet R. H. D., Smale A. P., Menzies J. W., Branduardi-Raymont G., Charles P. A., Mason K. O., Booth L., 1986, MNRAS, 221, 961
Davis L., Goldstein M., 1970, ApJ, 159, L81
Ftaclas C., Kearney M. W., Pechenick K., 1986, ApJ, 300, 203
Hellings P., de Loore C., 1986, A&A, 161, 75
Hut P., 1981, A&A, 99, 126
Hutchings J. B., 1974, ApJ, 192, 685
Janot-Pacheco E., Chevalier C., Ilovaisky S. A., 1982, in Jaschek M., Groth H., eds, IAU Symp. 98, Be Stars. Reidel, Dordrecht, p. 151
Kanno S., 1980, PASJ, 32, 105
Kemp J. C., Barbour M. S., 1983, ApJ, 264, 237
Leahy D. A., 1990, MNRAS, 242, 188 (L90)
Leahy D. A., 1991, MNRAS, 251, 203
Lyne A. G., Manchester R. N., 1988, MNRAS, 234, 477
Lyubarskii Y. E., Sunyaev R. A., 1988, Sov. Astron. Lett., 14, 390
McClintock J. E. et al., 1976, ApJ, 206, L99
Mészáros P., Bonazzola S., 1981, ApJ, 251, 695
Mészáros P., Nagel W., 1985, ApJ, 299, 138
Nagase F., Hayakawa S., Sato N., Masai K., Inoue H., 1986, PASJ, 38, 547
Pechenick K. R., Ftaclas C., Cohen J. M., 1983, ApJ, 274, 846
Rappaport S., Joss P. C., Stothers R., 1980, ApJ, 235, 570
Raubenheimer B. C., Ögelman H., 1990, A&A, 230, 73
Rothschild R. E. et al., 1979, Space Sci. Instr., 4, 269
Sato N., Nagase F., Kawai N., Kelley R. L., Rappaport S., White N. E., 1986, ApJ, 304, 241
Sheffer E. K. et al., 1992, SvA, 36, 41

APPENDIX

Let us generalize equation (1) by assuming for $f(\theta)$ a general expansion in terms of even powers of $\cos\theta$,

$$f(\theta)\approx\sum_{n=0}^{N}a_n\cos^{2n}(\theta). \tag{A1}$$

By means of equation (2) it is possible to express f as a function of the pulse phase φ:

$$f(\varphi)=\sum_{n=0}^{N}a_n\sum_{k=0}^{2n}b_k\cos^k(\varphi), \tag{A2}$$

where we have defined the coefficients b_k as

$$b_k\equiv\binom{2n}{k}A^{2n-k}B^k,$$

and A and B are defined as

$$A=\cos(\theta_1)\cos(\theta_2),\qquad B=\sin(\theta_1)\sin(\theta_2). \tag{A3}$$

After some algebra, we can rewrite equation (A2) as

$$\begin{aligned}f(\varphi)&=\sum_{n=0}^{N}a_n\left\{\sum_{k=1}^{n}b_{2k-1}\frac{1}{2^{2k-2}}\sum_{m=0}^{k-1}\binom{2k-1}{m}\cos(2k-2m-1)\varphi\right.\\&\left.+\sum_{k=0}^{n}b_{2k}\left[\frac{1}{2^{2k}}\binom{2k}{k}+\frac{1}{2^{2k-1}}\sum_{m=0}^{k-1}\binom{2k}{m}\cos(2k-2m)\varphi\right]\right\}.\end{aligned} \tag{A4}$$

Now let us discuss the particular solution in which one of the two angles in equation (A3) is close to $\pi/2$. In this case, we can Taylor-expand $\cos(\theta_1)$ around $\xi\equiv\pi/2-\theta_1$, and will consider only terms up to the second order:

$$\cos(\theta_1)\approx\xi+O(\xi^2),\qquad \sin(\theta_1)\approx\left(1-\frac{1}{2}\xi^2\right)+O(\xi^2).$$

With this approximation, the coefficients A and B can be written

$$\begin{aligned}A&\approx\xi\cos(\theta_1)\equiv\xi\cos\theta,\\B&\approx\left(1-\frac{1}{2}\xi^2\right)\sin(\theta_1)\equiv\left(1-\frac{1}{2}\xi^2\right)\sin\theta.\end{aligned} \tag{A5}$$

The powers of the coefficients A and B become

$$A^k=\begin{cases}\xi^k\cos^k\theta & k=0,1,2,\\0 & k>2,\end{cases}\qquad B^k=\left(1-\frac{k}{2}\xi^2\right)\sin^k\theta. \tag{A6}$$

The fact that A^k is null for $k>2$ has the consequence that only three of the coefficients b_k are different from zero, namely b_{2n}, b_{2n-1} and b_{2n-2}.

After a bit of algebra we find that equation (A4) can be written

$$\begin{aligned}f(\varphi)=&\sum_{n=0}^{N}a_n\left(\frac{\sin^{2n}\theta}{2^{2n-3}}\right)\\&\times\left\{\frac{1}{2}\left[n(2n-1)\xi^2\cot^2\theta\binom{2n-2}{n-1}+\frac{1-n\xi^2}{4}\binom{2n}{n}\right]\right.\\&+n\xi\cot\theta\sum_{m=1}^{n}\binom{2n-1}{n-m}\cos(2m-1)\varphi\\&+\sum_{m=1}^{n}\left[n(2n-1)\xi^2\cot^2\theta\binom{2n-2}{n-m-1}\right.\\&\left.\left.+\frac{1-n\xi^2}{4}\binom{2n}{n-m}\right]\cos(2m)\varphi\right\}.\end{aligned} \tag{A7}$$

The power spectrum of equation (A7) becomes

$$\begin{aligned}P(f)=&\mathscr{A}\delta(f)+\sum_{m=1}^{N}\mathscr{B}_m\delta[f-(2m-1)f_0]\\&+\sum_{m=1}^{N}\mathscr{C}_m\delta[f-(2m)f_0],\end{aligned} \tag{A8}$$

where we have defined

$$\begin{aligned}\mathscr{A}\equiv&\left\{\sum_{n=0}^{N}a_n\left(\frac{\sin^{2n}\theta}{2^{2n-3}}\right)\frac{1}{2}\left[n(2n-1)\xi^2\cot^2\theta\binom{2n-2}{n-1}\right.\right.\\&\left.\left.+\frac{1-n\xi^2}{4}\binom{2n}{n}\right]\right\}^2,\\\mathscr{B}_m\equiv&\frac{1}{2}\left[\sum_{n=0}^{N}a_n\left(\frac{\sin^{2n}\theta}{2^{2n-3}}\right)n\xi\cot\theta\binom{2n-1}{n-m}\right]^2,\\\mathscr{C}_m\equiv&\frac{1}{2}\left\{\sum_{n=0}^{N}a_n\left(\frac{\sin^{2n}\theta}{2^{2n-3}}\right)\left[n(2n-1)\xi^2\cot^2\theta\binom{2n-2}{n-m-1}\right.\right.\\&\left.\left.+\frac{1-n\xi^2}{4}\binom{2n}{n-m}\right]\right\}^2.\end{aligned} \tag{A9}$$